

# Quantifying defects in graphene via Raman spectroscopy at different excitation energies

L. G. Cançado<sup>1</sup>, A. Jorio<sup>1</sup>, E. H. Martins Ferreira<sup>2</sup>, F. Stavale<sup>2</sup>, C. A. Achete<sup>2</sup>, R. B. Capaz<sup>3</sup>, M. V. O. Moutinho<sup>3</sup>, A. Lombardo<sup>4</sup>, T. Kulmala<sup>4</sup>, and A. C. Ferrari<sup>4</sup>  
<sup>1</sup>*Departamento de Física, Universidade Federal de Minas Gerais, 30123-970, Belo Horizonte, Brazil*  
<sup>2</sup>*Divisão de Metrologia de Materiais, Instituto Nacional de Metrologia, Normalização e Qualidade Industrial (INMETRO), Duque de Caxias, RJ 25250-020, Brazil,*  
<sup>3</sup>*Instituto de Física, Universidade Federal do Rio de Janeiro, Cx. Postal 68528, Rio de Janeiro, 21941-972 RJ, Brazil, and*  
<sup>4</sup>*Department of Engineering, University of Cambridge, Cambridge CB3 0FA, UK.*

We present a Raman study of Ar<sup>+</sup>-bombarded graphene samples with increasing ion doses. This allows us to have a controlled, increasing, amount of defects. We find that the ratio between the D and G peak intensities for a given defect density strongly depends on the laser excitation energy. We quantify this effect and present a simple equation for the determination of the point defect density in graphene via Raman spectroscopy for any visible excitation energy. We note that, for all excitations, the D to G intensity ratio reaches a maximum for an inter-defect distance  $\sim 3$  nm. Thus, a given ratio could correspond to two different defect densities, above or below the maximum. The analysis of the G peak width and its dispersion with excitation energy solves this ambiguity.

## I. INTRODUCTION

Quantifying defects in graphene related systems, which include a large family of  $sp^2$  carbon structures, is crucial both to gain insight in their fundamental properties, and for applications. In graphene, this is a key step towards the understanding of the limits to its ultimate mobility<sup>1-3</sup>. Large efforts have been devoted to quantify defects and disorder using Raman spectroscopy for nanographites<sup>4-19</sup>, amorphous carbons<sup>17-23</sup>, carbon nanotubes<sup>24,25</sup>, and graphene<sup>11,26-34</sup>. The first attempt was the pioneering work of Tuinstra and Koenig (TK)<sup>4</sup>. They reported the Raman spectrum of graphite and nano-crystalline graphite, and assigned the mode at  $\sim 1580\text{cm}^{-1}$  to the high frequency  $E_{2g}$  Raman allowed optical phonon, now known as G peak<sup>5</sup>. In defected and nanocrystalline samples they measured a second peak at  $\sim 1350\text{cm}^{-1}$ , now known as D peak<sup>5</sup>. They assigned it to an  $A_{1g}$  breathing mode at the Brillouin Zone (BZ) boundary  $\mathbf{K}$ , activated by the relaxation of the Raman fundamental selection rule  $\mathbf{q} \approx \mathbf{0}$ , where  $\mathbf{q}$  is the phonon wavevector<sup>4</sup>. They noted that the ratio of the D to G intensities varied inversely with the crystallite size,  $L_a$ . Ref.<sup>17</sup> noted the failure of the TK relation for high defect densities, and proposed a more complete amorphization trajectory valid to date. Refs.<sup>7,8,17,18</sup> reported a significant excitation energy dependence of the intensity ratio. Refs.<sup>9,10</sup> measured this excitation laser energy dependency in the Raman spectra of nanographites, and the ratio between the D and G bands was shown to depend on the fourth power of the excitation laser energy  $E_L$ .

There is, however, a fundamental geometric difference between defects related to the size of a nano-crystallite and point defects in the  $sp^2$  carbon lattices, resulting in a different intensity ratio dependence on the amount of disorder. Basically, the amount of disorder in a

nano-crystallite is given by the amount of border (one-dimensional defects) with respect to the total crystallite area, and this is a measure of the nano-crystallite size  $L_a$ . In graphene with zero-dimensional point-like defects, the distance between defects,  $L_D$ , is a measure of the amount of disorder, and recent experiments show that different approaches must be used to quantify  $L_D$  and  $L_a$  by Raman spectroscopy<sup>27</sup>. The effect of changing  $L_D$  on peak width, frequency, intensity, and integrated area for many Raman peaks in single layer graphene was studied in Ref.<sup>28</sup>, and extended to N-layer graphene in Ref.<sup>29</sup>, all using a single laser line  $E_L = 2.41\text{eV}$ .

Here, to fully accomplish the protocol for quantifying point-like defects in graphene using Raman spectroscopy (or equivalently,  $L_D$ ), we use different excitation laser lines in ion-bombarded samples and measure the D to G peak intensity ratio. This ratio is denoted in literature as  $I_D/I_G$  or  $I(D)/I(G)$ , while the ratio of their areas, i.e. frequency integrated intensity, as  $A_D/A_G$  or  $A(D)/A(G)$ . In principle, for small disorder or perturbations, one should always consider the area ratio, since the area under each peak represents the probability of the whole process, considering uncertainty<sup>28,35</sup>. However, for large disorder, it is far more informative to decouple the information on peak intensity and full width at half maximum. The latter, denoted in literature as FWHM or  $\Gamma$ , is a measure of structural disorder<sup>10,21,28</sup>, while the intensity represents the phonon modes/molecular vibrations involved in the most resonant Raman processes<sup>17,18,21</sup>. For this reason, in this paper we will consider the decoupled  $I_D/I_G$  and peak widths trends. We find that, for a given  $L_D$ ,  $I_D/I_G$  increases as the excitation laser energy increases. We present a set of empirical formulas that can be used to quantify the amount of point-like defects in graphene samples with  $L_D \geq 10\text{nm}$  using any excitation laser energy/wavelength in the visible range. The analysis of the D and G peak widths and their dispersions with excita-

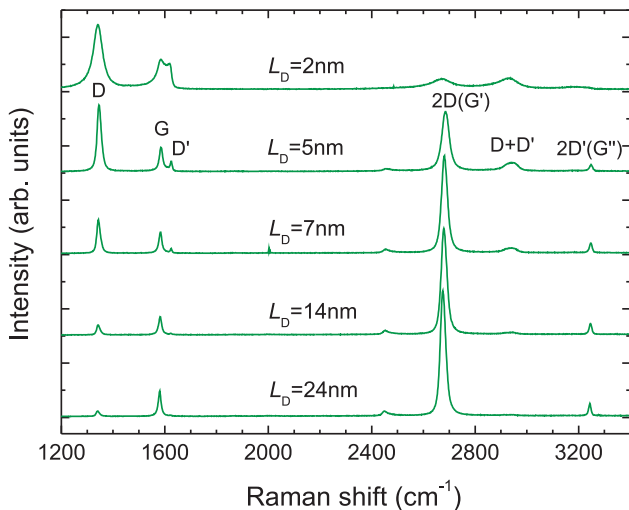


FIG. 1. Raman spectra of five ion bombarded SLG measured at  $E_L = 2.41$  eV ( $\lambda_L = 514.5$  nm). The  $L_D$  values are given according to Ref.<sup>27</sup>, and the main peaks are labeled. The notation within parenthesis [e.g.  $2D(G')$ ] indicate two commonly used notations for the same peak ( $2D$  and  $G'$ )<sup>30,40</sup>.

tion energy unambiguously discriminate between the two main stages of disordering incurred by such samples.

## II. RESULTS AND DISCUSSION

We produce single layer graphene (SLG) samples with increasing defect density by mechanical exfoliation followed by  $\text{Ar}^+$ -bombardment, as for the procedure outlined in Ref.<sup>27</sup>. The ion-bombardment experiments are carried out in an OMICRON VT-STM ultra-high vacuum system (base pressure  $5 \times 10^{-11}$  mbar) equipped with an ISE 5 Ion Source. Raman spectra are measured at room temperature with a Renishaw microspectrometer. The spot size is  $\sim 1 \mu\text{m}$  for a  $100\times$  objective, and the power is kept at  $\sim 1.0$  mW to avoid heating. The excitation energies,  $E_L$ , (wavelengths,  $\lambda_L$ ) are: Ti-Sapph 1.58 eV (785 nm), He-Ne 1.96 eV (632.8 nm),  $\text{Ar}^+$  2.41 eV (514.5 nm).

Figure 1 plots the Raman spectra of five SLG exposed to different ion bombardment doses in the range  $10^{11}$   $\text{Ar}^+/\text{cm}^2$  (one defect per  $4 \times 10^4$  C atoms) to  $10^{15}$   $\text{Ar}^+/\text{cm}^2$  (one defect for every four C atoms). The bombardment procedure described in Ref.<sup>27</sup> is accurately reproducible. By tuning the bombardment exposure we generated samples with  $L_D = 24, 14, 13, 7, 5$ , and 2 nm. All spectra in Fig. 1 are taken at  $E_L = 2.41$  eV ( $\lambda_L = 514.5$  nm).

The Raman spectra in Figure 1 consist of a set of dis-

tinct peaks. The G and D appear around  $1580 \text{ cm}^{-1}$  and  $1350 \text{ cm}^{-1}$ , respectively. The G peak corresponds to the  $E_{2g}$  phonon at the Brillouin zone center. The D peak is due to the breathing modes of six-atom rings and requires a defect for its activation<sup>4,17,18,36</sup>. It comes from transverse optical (TO) phonons around the  $\mathbf{K}$  or  $\mathbf{K}'$  points in the 1<sup>st</sup> Brillouin zone<sup>4,17,18</sup>, involves an intervalley double resonance process<sup>36,37</sup>, and is strongly dispersive<sup>38</sup> with excitation energy due to a Kohn Anomaly at  $\mathbf{K}^39$ . Double resonance can also happen as intravalley process, i. e. connecting two points belonging to the same cone around  $\mathbf{K}$  or  $\mathbf{K}'$ <sup>37</sup>. This gives the so-called  $D'$  peak, which is centered at  $\sim 1620 \text{ cm}^{-1}$  in defected samples measured at 514.5 nm<sup>12</sup>. The  $2D$  peak (also called  $G'$  in the literature) is the second order of the D peak<sup>12,30</sup>. This is a single peak in single layer graphene, whereas it splits in four in bilayer graphene, reflecting the evolution of the electron band structure<sup>30,40</sup>. The  $2D'$  peak (also called  $G''$  in analogy to  $G'$ ) is the second order of  $D'$ . Since  $2D(G')$  and  $2D'(G'')$  originate from a process where momentum conservation is satisfied by two phonons with opposite wavevectors, no defects are required for their activation, and are thus always present. On the other hand, the  $D + D'$  band ( $\sim 2940 \text{ cm}^{-1}$ ) is the combination of phonons with different momenta, around  $\mathbf{K}$  and  $\Gamma$ , thus requires a defect for its activation.

Ref.<sup>17</sup> proposed a three stage classification of disorder in carbon materials, to simply assess the Raman spectra of carbons along an amorphization trajectory leading from graphite to tetrahedral amorphous carbon: 1) graphite to nanocrystalline graphite; 2) nanocrystalline graphite to low  $sp^3$  amorphous carbon; 3) low  $sp^3$  amorphous carbon to high  $sp^3$  (tetrahedral) amorphous carbon. In the study of graphene, stages 1 and 2 are the most relevant and are summarized here.

In stage 1, the Raman spectrum evolves as follows<sup>17,27,28</sup>: a) D appears and  $I_D/I_G$  increases; b)  $D'$  appears; c) all peaks broaden. In the case of graphite the D and  $2D$  lose their doublet structure<sup>17,41</sup>; e)  $D + D'$  appears; f) at the end of stage 1, G and  $D'$  are so wide that they start to overlap. If a single lorentzian is used to fit  $G + D'$ , this results in an upshifted wide G band at  $\sim 1600 \text{ cm}^{-1}$ .

In stage 2, the Raman spectrum evolves as follows<sup>17</sup>: a) the G peak position, denoted in literature as  $\text{Pos}(G)$  or  $\omega_G$ , decreases from  $\sim 1600 \text{ cm}^{-1}$  towards  $\sim 1510 \text{ cm}^{-1}$ ; b) the TK relation fails and  $I_D/I_G$  decreases towards 0; c)  $\omega_G$  becomes dispersive with the excitation laser energy, the dispersion increasing with disorder; d) there are no more well defined second-order peaks, but a small modulated bump from  $\sim 2300 \text{ cm}^{-1}$  to  $\sim 3200 \text{ cm}^{-1}$ <sup>17,28</sup>.

In disordered carbons  $\omega_G$  increases as the excitation wavelength decreases, from IR to UV<sup>17</sup>. The dispersion rate,  $\text{Disp}(G) = \Delta\omega_G/\Delta E_L$ , increases with disorder. The G dispersion separates the materials into two types. In those with only  $sp^2$  rings,  $\text{Disp}(G)$  saturates at  $\sim 1600 \text{ cm}^{-1}$ , the G position at the end of stage 1. In contrast, for those containing  $sp^2$  chains (such as in amor-

phous and diamond-like carbons), G continues to rise past  $1600\text{ cm}^{-1}$  and can reach  $\sim 1690\text{ cm}^{-1}$  for  $229\text{ nm}$  excitation<sup>17,18</sup>. On the other hand, D always disperses with excitation energy<sup>17,18</sup>.  $\Gamma_G$  always increases with disorder<sup>10,23,27,28</sup>. Thus, combining  $I_D/I_G$  and  $\Gamma_G$  allows to discriminate between stages 1 or 2, since samples in stage 1 and 2 could have the same  $I_D/I_G$ , but not the same  $\Gamma_G$ , being this much bigger in stage 2<sup>23,27,28</sup>.

We note that Figure 1 shows the loss of sharp second order features in the Raman spectrum obtained from the  $L_D = 2\text{ nm}$  SLG. This is an evidence that the range of defect densities in our study covers stage 1 (samples with  $L_D = 24, 14, 13, 7, 5\text{ nm}$ ) and the onset of stage 2 (sample with  $L_D = 2\text{ nm}$ ).

Figures 2a-c report the first-order Raman spectra of our ion-bombarded SLGs measured at  $E_L = 1.58\text{ eV}$  ( $\lambda_L = 785\text{ nm}$ ),  $1.96\text{ eV}$  ( $632.8\text{ nm}$ ),  $2.41\text{ eV}$  ( $514.5\text{ nm}$ ), respectively. Figure 2d shows the Raman spectra of the ion-bombarded SLG with  $L_D = 7\text{ nm}$  obtained using the three different laser energies. We note that  $I_D/I_G$  considerably changes with the excitation energy. This is a well-know effect in the Raman scattering of  $sp^2$  carbons<sup>9,10,17,18,42,43</sup>. Ref.<sup>10</sup> noted that the integrated areas of different peaks depend differently on excitation energy  $E_L$ : while  $A_D$ ,  $A_{D'}$ , and  $A_{2D}$  shown no  $E_L$ -dependence,  $A_G$  was found to be proportional to  $E_L^4$ . The independence of  $A_{2D}$  on  $E_L$  agrees with the theoretical prediction<sup>44</sup> if one assumes that the electronic scattering rate is proportional to the energy. However, a fully quantitative theory is not trivial since, in general,  $A_D$  depends not only on the concentration of defects, but on their type as well (e.g., only defects able to scatter electrons between the two valleys can contribute)<sup>31,32,34</sup>. Different defects can also produce different frequency and polarization dependence of  $A_D$ <sup>31,32,34</sup>.

Figure 3 plots  $I_D/I_G$  for all SLGs and laser energies. For all  $E_L$ ,  $I_D/I_G$  increases as  $L_D$  decreases (stage 1), reaches a maximum at  $L_D \sim 3\text{ nm}$ , and decreases towards zero for  $L_D < 3\text{ nm}$  (stage 2). It is important to understand what the maximum of  $I_D/I_G$  vs.  $L_D$  means.  $I_D$  will keep increasing until the contribution from each defect sums independently<sup>27,31</sup>. In this regime (stage 1)  $I_D$  is proportional to the total number of defects probed by the laser spot. For an average defect distance  $L_D$  and laser spot size  $L_L$ , there are on average  $(L_L/L_D)^2$  defects in the area probed by the laser, thus  $I_D \propto (L_L/L_D)^2$ . On the other hand,  $I_G$  is proportional to the total area probed by the laser  $\propto L_L^2$ , giving  $I_D/I_G \propto 1/L_D^2$ <sup>17,27</sup>. However, if two defects are closer than the average distance an e-h pair travels before scattering with a phonon, then their contributions will not sum independently anymore<sup>27,28,31,33</sup>. This distance can be estimated as  $v_F/\omega_D \sim 3\text{ nm}$ <sup>31</sup>, where  $v_F \sim 10^6\text{ m/s}$  is the Fermi velocity around the  $\mathbf{K}$  and  $\mathbf{K}'$  points, in excellent agreement with the predictions of Refs.<sup>17</sup> and the data of Refs.<sup>27,28,33</sup>. For an increasing number of defects (stage 2), where  $L_D < 3\text{ nm}$ ,  $sp^2$  domains become smaller and the rings fewer and more distorted, until they open

up. As the G peak is just related to the relative motion of  $sp^2$  carbons, we can assume  $I_G$  roughly constant as a function of disorder. Thus, with the loss of  $sp^2$  rings,  $I_D$  will decrease with respect to  $I_G$  and the  $I_D/I_G \propto 1/L_D^2$  relation will no longer hold. In this regime,  $I_D/I_G \propto M$  ( $M$  being the number of ordered rings), and the development of a D peak indicates ordering, exactly the opposite to stage 1<sup>17</sup>. This leads to a new relation:  $I_D/I_G \propto L_D^2$ <sup>17</sup>.

The solid lines in Fig. 3 are fitting curves following the relation proposed in Ref.<sup>27</sup>:

$$\frac{I_D}{I_G} = C_A \frac{(r_A^2 - r_S^2)}{(r_A^2 - 2r_S^2)} \left[ e^{-\pi r_S^2/L_D^2} - e^{-\pi(r_A^2 - r_S^2)/L_D^2} \right]. \quad (1)$$

The parameters  $r_A$  and  $r_S$  are length scales which determine the region where the D band scattering takes place.  $r_S$  determines the radius of the structurally disordered area caused by the impact of an ion.  $r_A$  is defined as the radius of the area surrounding the point defect in which the D band scattering takes place, although the  $sp^2$  hexagonal structure is preserved<sup>27</sup>. In short, the difference  $r_A - r_S$  defines the Raman relaxation length of the D band scattering, and is associated with the coherence length of electrons which undergo inelastic scattering by optical phonons<sup>27,33</sup>. The fit in Figure 2 is done considering  $r_S = 1\text{ nm}$  (as determined in Ref.<sup>27</sup> and expected to be a structural parameter, i.e.  $E_L$  independent). Furthermore, within experimental accuracy, all data can be fit with the same  $r_A = 3.1\text{ nm}$ , in excellent agreement with the values obtained in Refs.<sup>27,28,33</sup>. Any uncertainty in  $r_A$  does not affect the results in the low defect density regime ( $L_D > 10\text{ nm}$ ) discussed later.

Ref.<sup>27</sup> suggested that  $I_D/I_G$  depends on both an activated (A) area, pounded by the parameter  $C_A$ , and a structurally defective area (S), pounded by a parameter  $C_S$ . Here we selected  $C_S = 0$  in eq. (1) for two reasons: (i)  $C_S$  should be defect-structure dependent, and in the ideal case where the defect is the break-down of the C-C bonds,  $C_S$  should be null; (ii) here we do not focus on the large defect density regime,  $L_D < r_S$ . The parameter  $C_A$  in eq. (1) corresponds to the maximum possible  $I_D/I_G$ , which would be observed in the ideal situation where the D band would be activated in the entire sample with no break down of any hexagonal carbon ring<sup>27</sup>.

$C_A$  has been addressed in Ref.<sup>27</sup> as related to the ratio between the scattering efficiency of optical graphene phonons evaluated between  $\Gamma$  and  $\mathbf{K}$ . As we show here, the large  $I_D/I_G$  dependence on  $E_L$  comes from the change on  $C_A$ , which suggests this parameter might also depend on interference effects, when summing the different electron/hole scattering processes that are possible when accounting for the Raman cross section<sup>45-49</sup>. Note that  $C_A$  decreases as the laser energy increases. The solid line in the inset to Fig. 2 is the fit of the experimental data (dark squares) by using an empirical relation between the maximum value of  $I_D/I_G$  and  $E_L$ , of the form  $C_A = A E_L^{-B}$ . The fit yields  $A = (160 \pm 48)\text{ eV}^4$ , by setting  $B = 4$  in agreement with Refs.<sup>9,10</sup>.

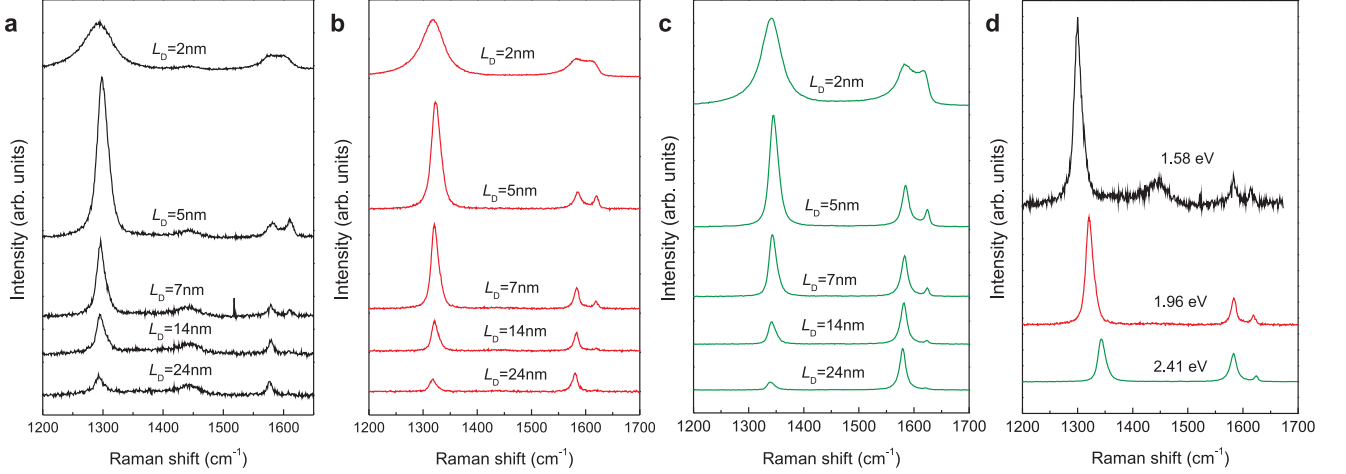


FIG. 2. (a-c) Raman spectra of five distinct ion-bombarded graphene samples using the excitation laser energies (wavelengths)  $E_L = 1.58$  eV ( $\lambda_L = 785$  nm),  $E_L = 1.96$  eV ( $\lambda_L = 632.8$  nm), and  $E_L = 2.41$  eV ( $\lambda_L = 514.5$  nm), respectively. (d) Raman spectra of an ion-bombarded sample with  $L_D = 7$  nm obtained using these three excitation laser energies.

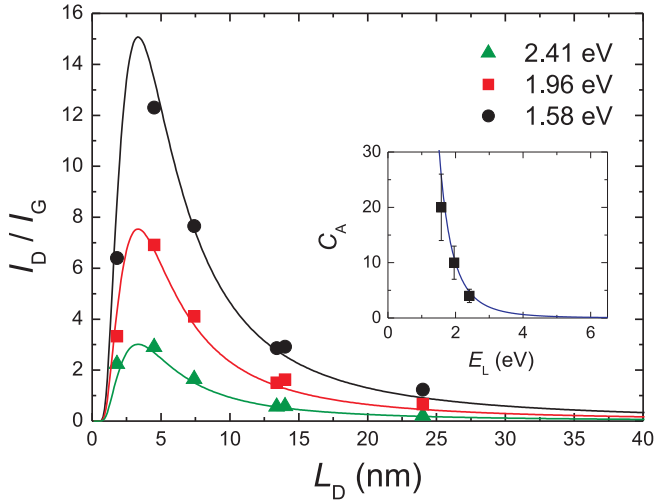


FIG. 3.  $I_D/I_G$  for all samples and laser energies considered here. Solid lines are fits according to equation 1 with  $r_S = 1$  nm,  $C_S = 0$ , and  $r_A = 3.1$  nm. The inset plots  $C_A$  as a function of  $E_L$ . The solid curve is given by  $C_A = (160 \pm 48) E_L^{-4}$ .

We now focus on the low-defect density regime ( $L_D \geq 10$  nm), since this is the case of most interest in order to understand how Raman active defects limit the ultimate mobility of graphene samples<sup>1-3</sup>. In this regime, where  $L_D > 2r_A$ , the total area contributing to the D band scattering is proportional to the number of point defects, giving rise to  $I_D/I_G \propto 1/L_D^2$ , as discussed above. For

large values of  $L_D$ , eq. (1) can be approximated to

$$\frac{I_D}{I_G} \simeq C_A \frac{\pi(r_A^2 - r_S^2)}{L_D^2}. \quad (2)$$

By taking  $r_A = 3.1$  nm,  $r_S = 1$  nm, and also the relation  $C_A = (160 \pm 48) E_L^{-4}$  obtained from the fit of the experimental data shown in Figure 2, eq. (2) can be rewritten as

$$L_D^2 (\text{nm}^2) = \frac{(4.3 \pm 1.3) \times 10^3}{E_L^4} \left( \frac{I_D}{I_G} \right)^{-1}. \quad (3)$$

In terms of excitation laser wavelength  $\lambda_L$  (in nanometers), we have

$$L_D^2 (\text{nm}^2) = (1.8 \pm 0.5) \times 10^{-9} \lambda_L^4 \left( \frac{I_D}{I_G} \right)^{-1}. \quad (4)$$

Equations (3) and (4) are valid for Raman data obtained from graphene samples with point defects separated by  $L_D \geq 10$  nm using excitation lines in the visible range. In terms of defect density  $n_D (\text{cm}^{-2}) = 10^{14} / (\pi L_D^2)$ , eqs. (3) and (4) become

$$n_D (\text{cm}^{-2}) = (7.3 \pm 2.2) \times 10^9 E_L^4 \left( \frac{I_D}{I_G} \right), \quad (5)$$

and

$$n_D (\text{cm}^{-2}) = \frac{(1.8 \pm 0.5) \times 10^{22}}{\lambda_L^4} \left( \frac{I_D}{I_G} \right). \quad (6)$$

Figure 4 plots  $E_L^4 (I_D/I_G)$  as a function of  $L_D$  for the data shown in Figure 2. The data with  $L_D > 10$  nm obtained with different laser energies collapse in the same

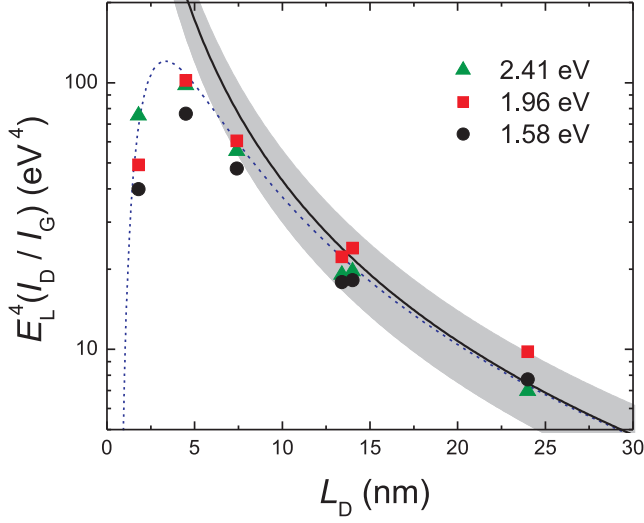


FIG. 4.  $E_L^4(I_D/I_G)$  as a function of  $L_D$  for the data shown in Figure 2. The dashed blue line is the plot obtained from the substitution of the relation  $C_A = (160)/E_L^4$  in equation 1. The solid dark line is the plot of the product  $E_L^4(I_D/I_G)$  as a function of  $L_D$  according to equation 3. The shadow area accounts for the upper and lower limits given by the  $\pm 30\%$  experimental error.

curve. The dashed blue line is the plot obtained from the substitution of the relation  $C_A = (160)/E_L^4$  in eq. 1. The solid dark line is the plot  $E_L^4(I_D/I_G)$  versus  $L_D$  according to eqs. (3) and (4). The shadow area accounts for the upper and lower limits given by the  $\pm 30\%$  experimental error. The plot in Fig. 4 validates these relations for samples with  $L_D > 10$  nm.

Figure 5a plots  $\Gamma_D$  and  $\Gamma_{2D}$  as a function of  $L_D$ . Within the experimental error, a dependence of  $\Gamma_D$  or  $\Gamma_{2D}$  on the excitation energy during stage 1 can not be observed. D and 2D always disperse with excitation energy, with  $\Delta\omega_D/\Delta E_L \sim 52 \text{ cm}^{-1}/\text{eV}$ , and  $\Delta\omega_{2D}/\Delta E_L = 2\Delta\omega_D/\Delta E_L$ .

Figures 5b,c plot the G peak dispersion  $\text{Disp}(G) = \Delta\omega_G/\Delta E_L$  and  $\Gamma_G = \text{FWHM}(G)$  as a function of  $L_D$ , respectively. As shown in Figure 5b,  $\Delta\omega_G/\Delta E_L$  remains zero until the onset of stage two, when it becomes slightly dispersive ( $\Delta\omega_G/\Delta E_L \sim 6 \text{ cm}^{-1}/\text{eV}$ ).  $\Gamma_G$  (Figure 5c) remains roughly constant at  $\sim 14 \text{ cm}^{-1}$ , a typical value for as-prepared exfoliated graphene<sup>11,30,50,51</sup>, until the onset of stage 2 (corresponding to the maximum  $I_D/I_G$ ) as suggested in Ref.<sup>23</sup>, and shown in Ref.<sup>28</sup> for a single laser line  $E_L = 2.41 \text{ eV}$ . Combining  $I_D/I_G$  and  $\Gamma_G$  allows to discriminate between stages 1 or 2, since samples in stage 1 and 2 could have the same  $I_D/I_G$ , but not the same  $\Gamma_G$ , which is much larger in stage 2<sup>23,28</sup>.

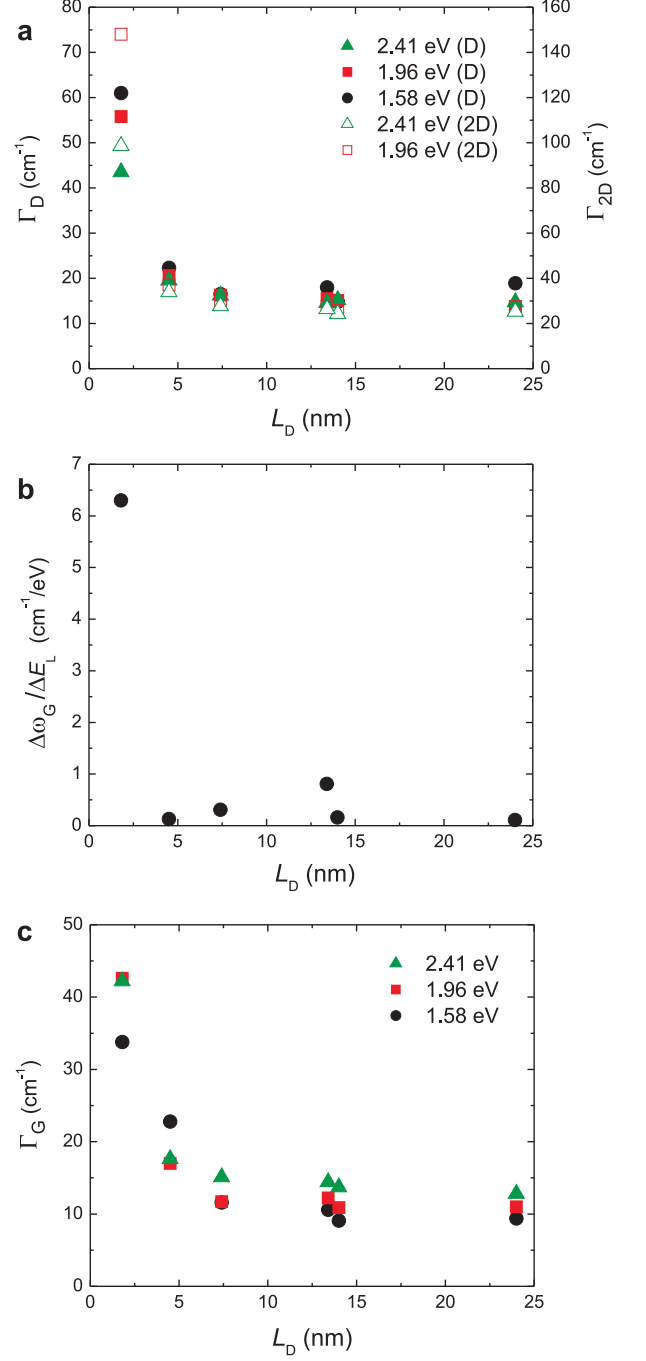


FIG. 5. (a) Plot of  $\Gamma_D$  and  $\Gamma_{2D}$  versus  $L_D$ . (b) G peak dispersion [ $\text{Disp}(G) = \Delta\omega_G/\Delta E_L$ ] as a function of  $L_D$ .  $\Delta\omega_G/\Delta E_L$  remains zero until the onset of stage 2. (c)  $\text{FWHM}(G) = \Gamma_G$  as a function of  $L_D$ . As suggested in Refs.<sup>23,28</sup>,  $\Gamma_G$  remains roughly constant until the onset of the second stage of amorphization, corresponding to the maximum  $I_D/I_G$ .

### III. CONCLUSIONS

In summary, we discussed the use of Raman spectroscopy for quantifying the amount of point-like defects in graphene. We used different excitation laser lines in ion-bombarded samples in order to measure their respective  $I_D/I_G$ . We find that  $I_D/I_G$ , for a specific  $L_D$ , depends on the laser energy. We presented a set of empirical relations that can be used to quantify point defects in graphene samples with  $L_D > 10$  nm via Raman spectroscopy using any laser line in the visible range. We show that the Raman coherence length  $r_A$  is  $E_L$ -independent, while the strong  $E_L$  dependence for  $I_D/I_G$

comes from the parameter  $C_A$ .

### IV. ACKNOWLEDGEMENTS

We acknowledge funding from a Royal Society International Project Grant. ACF acknowledges funding from ERC grant NANOPOTS, EPSRC grant EP/G042357/1, a Royal Society Wolfson Research Merit Award, EU grants RODIN and Marie Curie ITN-GENIUS (PITN-GA-2010-264694), and Nokia Research Centre, Cambridge. LGC and AJ acknowledge the support from the Brazilian agencies CNPq and FAPEMIG. EHMf, FS, and CAA acknowledge financial support from Inmetro.

- 
- <sup>1</sup> Z. Ni, L. Ponomarenko, R. Nair, R. Yang, S. Anissimova, I. Grigorieva, F. Schedin, P. Blake, Z. Shen, E. Hill, K. S. Novoselov, and A. K. Geim, "On resonant scatterers as a factor limiting carrier mobility in graphene". *Nano Lett.* **10**, 3868-3872 (2010).
  - <sup>2</sup> J. H. Chen, W. G. Cullen, C. Jang, M. S. Fuhrer, and E. D. Williams, "Defect scattering in graphene". *Phys. Rev. Lett.* **102**, 236805-236808 (2008).
  - <sup>3</sup> C. R. Dean, A. F. Young, I. Meric, C. Lee, L. Wang, S. Sorgenfrei, K. Watanabe, T. Taniguchi, P. Kim, K. L. Shepard, and J. Hone, "Boron nitride substrates for high-quality graphene electronics". *Nature Nanotech.* **5**, 722-726 (2010).
  - <sup>4</sup> F. Tuinstra, and J. L. Koenig, "Raman spectrum of graphite". *J. Phys. Chem.* **53**, 1126-1130 (1970).
  - <sup>5</sup> R. Vidano, and D. B. Fischbach, "New lines in the Raman spectra of carbon and graphite". *J. Am. Ceram. Soc.* **61**, 13-17 (1978).
  - <sup>6</sup> D. S. Knight, and W. B. White, "Characterization of diamond films by Raman spectroscopy". *J. Mater. Res.* **4**, 385-393 (1989).
  - <sup>7</sup> K. Sinha, and J. Menendez, "First- and second-order resonant Raman scattering in graphite". *Phys. Rev. B* **41**, 10845-10847 (1990).
  - <sup>8</sup> M. J. Matthews, M. A. Pimenta, G. Dresselhaus, M. S. Dresselhaus, and M. Endo, "Origin of dispersive effects of the Raman D band in carbon materials". *Phys. Rev. B* **59**, (R)6585-(R)6588 (1999).
  - <sup>9</sup> L. G. Cançado, K. Takai, T. Enoki, M. Endo, Y. A. Kim, H. Mizusaki, A. Jorio, L. N. Coelho, R. Magalhães-Paniago, and M. A. Pimenta. "General equation for the determination of the crystallite size  $L_a$  of nanographite by Raman spectroscopy". *Appl. Phys. Lett.* **88**, 3106-3109 (2006).
  - <sup>10</sup> L. G. Cançado, A. Jorio, and M. A. Pimenta. "Measuring the absolute Raman cross section of nanographites as a function of laser energy and crystallite size". *Phys. Rev. B* **76**, 064304-064310 (2007).
  - <sup>11</sup> A. C. Ferrari, "Raman spectroscopy of graphene and graphite: Disorder, electron-phonon coupling, doping and nonadiabatic effects". *Solid State Comm.* **143**, 47-57 (2007).
  - <sup>12</sup> R. J. Nemanich, S. A. Solim, "First- and second-order Raman scattering from finite-size crystals of graphite". *Phys. Rev. B* **20**, 392-401 (1979).
  - <sup>13</sup> P. Lespade, A. Marchard, M. Couzi, and F. Cruege, "Caracterisation de materiaux carbonés par microspectrometrie Raman". *Carbon* **22**, 375-385 (1984).
  - <sup>14</sup> A. Cuesta, P. Dhamelincourt, J. Laureyns, A. Martinez-Alonso, J. M. D. Tascon, "Comparative performance of X-ray diffraction and Raman microprobe techniques for the study of carbon materials". *J. Mater. Chem.* **8**, 2875-2879 (1998).
  - <sup>15</sup> H. Wilhem, M. Lelaurain, E. McRae, and B. Humbert, "Raman spectroscopic studies on well-defined carbonaceous materials of strong two-dimensional character". *J. Appl. Phys.* **84**, 6552-6558 (1998).
  - <sup>16</sup> M. A. Pimenta, G. Dresselhaus, M. S. Dresselhaus, L. G. Cançado, A. Jorio, and R. Saito, "Studying disorder in graphite-based systems by Raman spectroscopy". *Phys. Chem. Chem. Phys.* **9**, 1276-1291 (2007).
  - <sup>17</sup> A. C. Ferrari, and J. Robertson, "Interpretation of Raman spectra of disordered and amorphous carbon". *Phys. Rev. B* **61**, 14095-14107 (2000).
  - <sup>18</sup> A. C. Ferrari, and J. Robertson, "Resonant Raman spectroscopy of disordered, amorphous, and diamondlike carbon". *Phys. Rev. B* **64**, 075414-075426 (2001).
  - <sup>19</sup> A. C. Ferrari, J. Robertson (Eds.), "Raman spectroscopy in carbons: From nanotubes to diamond". *Philos. Trans. R. Soc. Ser. A* **362**, 2267 (2004).
  - <sup>20</sup> A. C. Ferrari, and J. Robertson, "Origin of the 1150  $\text{cm}^{-1}$  Raman mode in nanocrystalline diamond". *Phys. Rev. B* **63**, (R)121405-(R)121408 (2001).
  - <sup>21</sup> C. Casiraghi, A. C. Ferrari, and J. Robertson, "Raman spectroscopy of hydrogenated amorphous carbon". *Phys. Rev. B* **72**, 085401-085414 (2005).
  - <sup>22</sup> B. Racine, A. C. Ferrari, N. A. Morrison, I. Hutchings, W. I. Milne, and J. Robertson, "Properties of amorphous carbon-silicon alloys deposited by a high plasma density source". *J. Appl. Phys.* **90**, 5002-5012 (2001).
  - <sup>23</sup> A. C. Ferrari, S. E. Rodil, and J. Robertson, "Interpretation of infrared and Raman spectra of amorphous carbon nitrides". *Phys. Rev. B* **67**, 155306-155325 (2003).
  - <sup>24</sup> M. Hulman, V. Skakalova, S. Roth, and H. J. Kuzmany, "Raman spectroscopy of single-wall carbon nanotubes and graphite irradiated by  $\gamma$  rays". *J. Appl. Phys.* **98**, 024311-024315 (2005).

- <sup>25</sup> S. G. Chou, H. Son, J. Kong, A. Jorio, R. Saito, M. Zheng, G. Dresselhaus, and M. S. Dresselhaus, "Length characterization of DNA-wrapped carbon nanotubes using Raman spectroscopy". *Appl. Phys. Lett.* **90**, 131109-131111 (2007).
- <sup>26</sup> D. Teweldebrhan, and A. A. Baladin, "Modification of graphene properties due to electron-beam irradiation". *Appl. Phys. Lett.* **94**, 013101-013103 (2009).
- <sup>27</sup> M. M. Lucchese, F. Stavale, E. H. Martins Ferreira, C. Vilane, M. V. O. Moutinho, R. B. Capaz, C. A. Achete, and A. Jorio, "Quantifying ion-induced defects and Raman relaxation length in graphene", *Carbon* **48**, 1592-1597 (2010).
- <sup>28</sup> E. H. Martins Ferreira, M. V. O. Moutinho, F. Stavale, M. M. Lucchese, R. B. Capaz, C. A. Achete, and A. Jorio, "Evolution of the Raman spectra from single-, few-, and many-layer graphene with increasing disorder". *Phys. Rev. B* **82**, 125429-125437 (2010).
- <sup>29</sup> A. Jorio, M. M. Lucchese, F. Stavale, E. H. Martins Ferreira, M. V. O. Moutinho, R. B. Capaz, and C. A. Achete, "Raman study of ion-induced defects in N-layer graphene". *J. Phys.: Condens. Matter* **22**, 334204-334208 (2010).
- <sup>30</sup> A. C. Ferrari, J. C. Meyer, V. Scardaci, C. Casiraghi, M. Lazzeri, F. Mauri, S. Piscanec, D. Jiang, K. S. Novoselov, S. Roth, and A. K. Geim, "Raman spectrum of graphene and graphene layers". *Phys. Rev. Lett.* **97**, 187401-187403 (2006).
- <sup>31</sup> C. Casiraghi, A. Hartschuh, H. Qian, S. Piscanec, C. Georgi, A. Fasoli, K. S. Novoselov, D. M. Basko, and A. C. Ferrari. "Raman spectroscopy of graphene edges". *Nano Lett.* **9**, 1433-1441 (2009).
- <sup>32</sup> B. Krauss, P. Nemes-Incze, V. Skakalova, L. P. Biro, K. von Klitzing, and J. H. Smet, "Raman scattering at pure graphene zigzag edges". *Nano Lett.* **10**, 4544-4548 (2010).
- <sup>33</sup> R. Beams, L. G. Cançado, and L. Novotny, "Low temperature Raman study of the electron coherence length near graphene edges". *Nano Lett.* **11**, 1177-1181 (2011).
- <sup>34</sup> L. G. Cançado, M. A. Pimenta, B. R. A. Neves, M. S. Dantas, and A. Jorio, "Influence of the atomic structure on the Raman spectra of graphite edges". *Phys. Rev. Lett.* **93**, 247401-247404 (2004).
- <sup>35</sup> D. M. Basko, S. Piscanec, and A. C. Ferrari, "Electron-electron interactions and doping dependence of the two-phonon Raman intensity in graphene". *Phys. Rev. B* **80**, 165413-165422 (2009).
- <sup>36</sup> C. Thomsen, and S. Reich, "Double resonant Raman scattering in graphite". *Phys. Rev. Lett.* **85**, 5214-5217 (2000).
- <sup>37</sup> R. Saito, A. Jorio, A. G. Souza Filho, G. Dresselhaus, M. S. Dresselhaus, and M. A. Pimenta, "Probing phonon dispersion relations of graphite by double resonance Raman scattering". *Phys. Rev. Lett.* **88**, 027401-027404 (2001).
- <sup>38</sup> R. P. Vidano, D. B. Fishbach, L. J. Willis, and T. M. Loehr, "Observation of Raman band shifting with excitation wavelength for carbons and graphites". *Solid State Commun.* **39**, 341-344 (1981).
- <sup>39</sup> S. Piscanec, M. Lazzeri, F. Mauri, A. C. Ferrari, and J. Robertson, "Kohn anomalies and electron-phonon interactions in graphite". *Phys. Rev. Lett.* **93**, 185503-185506 (2004).
- <sup>40</sup> L. G. Cançado, A. Reina, J. Kong, and M. S. Dresselhaus, "Geometrical approach for the study of G' band in the Raman spectrum of monolayer graphene, bilayer graphene, and bulk graphite". *Phys. Rev. B* **77**, 245408-245416 (2008).
- <sup>41</sup> L. G. Cançado, K. Takai, T. Enoki, M. Endo, Y. A. Kim, H. Mizusaki, N. L. Speziali, A. Jorio, and M. A. Pimenta, "Measuring the degree of stacking order in graphite by Raman spectroscopy". *Carbon* **46**, 272-275 (2008).
- <sup>42</sup> I. Pocsik, M. Hundhausen, M. Koos, and L. Ley, "Origin of the D peak in the Raman spectrum of microcrystalline graphite". *J. Non-Cryst. Solids* **227-230**, 1083-1086 (1998).
- <sup>43</sup> T. P. Mernagh, R. P. Cooney, and R. A. Johnson, "Raman spectra of graphon carbon black". *Carbon* **22**, 39-42 (1984).
- <sup>44</sup> D. M. Basko, "Theory of resonant multiphonon Raman scattering in graphene". *Phys. Rev. B* **78**, 125418-125459 (2008).
- <sup>45</sup> J. Maultzsch, S. Reich, and C. Thomsen, "Double-resonant Raman scattering in graphite: Interference effects, selection rules, and phonon dispersion". *Phys. Rev. B* **70**, 155403-155411 (2004).
- <sup>46</sup> D. M. Basko, "Calculation of the Raman G peak intensity in monolayer graphene: role of Ward identities". *New J. Phys.* **11**, 095011-095022 (2009).
- <sup>47</sup> M. Kalbac, A. Reina-Cecco, H. Farhat, J. Kong, L. Kavan, and M. S. Dresselhaus, "The Influence of Strong Electron and Hole Doping on the Raman Intensity of Chemical Vapor-Deposition Graphene". *ACS Nano* **10**, 6055-6063 (2010).
- <sup>48</sup> C. F. Chen, C. H. Park, B. W. Boudouris, J. Horng, B. Geng, C. Girit, A. Zettl, M. F. Crommie, R. A. Segalan, S. G. Louie, and F. Wang, "Controlling inelastic light scattering quantum pathways in graphene". *Nature* **471**, 618-620 (2011).
- <sup>49</sup> P. Venzuela, M. Lazzeri, and F. Mauri, "Theory of double-resonant Raman spectra in graphene: intensity and line shape of defect-induced and two-phonon bands". arXiv:1103.4582 (2011).
- <sup>50</sup> S. Pisana, M. Lazzeri, C. Casiraghi, K. S. Novoselov, A. K. Geim, A. C. Ferrari, and F. Mauri, "Breakdown of the adiabatic Born-Oppenheimer approximation in graphene". *Nature Mat.* **6**, 198-201 (2007).
- <sup>51</sup> M. Lazzeri, S. Piscanec, F. Mauri, A. C. Ferrari, and J. Robertson, "Phonon linewidths and electron-phonon coupling in graphite and nanotubes". *Phys. Rev. B* **73**, 155426-155431 (2006).